2022-11

Deterministic and stochastic theory for a resonant triad

Andrade, D

10.1016/j.wavemoti.2022.103087
Wave Motion
Elsevier BV

Wave Motion 116 (2023) 103087

Contents lists available at ScienceDirect

Wave Motion

journal homepage: www.elsevier.com/locate/wamot

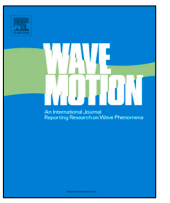

Deterministic and stochastic theory for a resonant triad

David Andrade, Raphael Stuhlmeier *

Center for Mathematical Sciences, University of Plymouth, PL4 8AA, UK

ARTICLE INFO

Article history:
Received 10 May 2022
Received in revised form 14 October 2022
Accepted 26 October 2022
Available online 9 November 2022

Keywords:
Wave–wave interaction
Triad resonance
Phase coherence
Phase-locking

ABSTRACT

We study a simple model of three resonantly-interacting nonlinear waves. Linear stability analysis allows for an easy identification of stable and unstable initial conditions. Subsequently, a reformulation of the problem allows us to establish the onset of phase coherence, demonstrating its critical role in the growth of instabilities. Furthermore, we are able to provide explicit expressions for the time-varying moments of the modal amplitudes, as well as for the bispectrum which measures phase coherence. We provide direct insight into the long-time statistics of the system without Monte-Carlo simulation. This includes long-time asymptotics, which show that the system desynchronises, leading to the convergence of the second order moments and decay in the bispectrum.

1. Introduction

Three-wave resonances occur in a variety of different physical contexts, from gravity-capillary waves [1–4], to plasmas [5], planetary waves [6] or the behaviour of an elastic pendulum [7]. Such resonances, which are driven by quadratic nonlinearity, are also mathematically attractive as the smallest possible set of waves which can undergo resonant energy exchange — this makes them a simpler stepping stone to the four, five, or six wave resonances which are encountered for certain dispersion relations (e.g. in deep water waves [8–10]).

The behaviour of our three-wave system can be described deterministically: one can linearise assuming an initially dominant mode, and find that the linear system allows for stable and unstable initial conditions. The full nonlinear system is also amenable to analysis by means of an exact solution: initial data lead either to blow-up in finite time, oscillation, or (for a degenerate case) to an oscillation with infinite period.

The analytic tractability of the system also allows us to obtain direct insight into the stochastic behaviour of the system, and how it responds to random variation in the phase. Normally such insight is restricted to linear systems, which can be explicitly solved and where each mode oscillates independently of the others. In such systems the distribution of energy among the modes never changes. For nonlinear systems, where interaction between Fourier modes gives rise to changes in energy, it is typically necessary to make approximations in order to study the averaged properties stemming, e.g. from an assumption of random initial phases (see e.g. [11,12] in the context of water waves).

In the present case, we are able to provide direct insight into the phase-averaged behaviour of a fundamentally nonlinear system by exploiting the explicit solution. For short-times it is observed that a linearly unstable configuration undergoes phase-locking, so that the dynamics are entirely independent of the initial phase. This high degree of coherence between the phases is exhibited in a fast initial evolution of the averaged modal energy. Correlations between the Fourier modes arise, and these can be measured using the bispectrum. The subsequent long-time behaviour of these correlations

* Corresponding author.
E-mail addresses: david.andrade@plymouth.ac.uk (D. Andrade), raphael.stuhlmeier@plymouth.ac.uk (R. Stuhlmeier).

https://doi.org/10.1016/j.wavemoti.2022.103087

can likewise be elucidated, and the bispectrum is shown to decay, the phases exhibiting a tendency towards decoherence. For long times, the averaged energy of the Fourier modes tends towards a constant value.

Throughout our analysis we are able to draw on Monte-Carlo simulations with random phases, which can be shown to match the averaged properties of the exact solutions. This provides both a valuable test case for approximations based on a random-phase approach, as well as a building block for understanding other resonant systems, including systems with more modes.

2. The three-wave equations

Our starting point is the system of three-wave equations

$$A_1' = s_1 A_2^* A_3^*, \tag{1a}$$
$$A_2' = s_2 A_1^* A_3^*, \tag{1b}$$
$$A_3' = s_3 A_1^* A_2^*, \tag{1c}$$

for the evolution of the complex amplitudes $A_i(t)$, and where s_i is assumed to be a real constant for $i = 1, 2, 3$. We consider this system in a generic context, but the interested reader can find derivations leading thereto in Craik [13] and the references therein. In particular, when such a system arises in the analysis of a particular physical system or partial differential equation, the coefficients s_i are determined by the physics, see [5,6].

A convenient reformulation is achieved when separating these complex amplitudes into (time-dependent) magnitudes and phases $A_i(t) = b_i(t)\exp(i\theta_i(t))$. Then we find:

$$b_1' = s_1 b_2 b_3 \cos(\theta), \tag{2a}$$
$$b_2' = s_2 b_1 b_3 \cos(\theta), \tag{2b}$$
$$b_3' = s_3 b_1 b_2 \cos(\theta), \tag{2c}$$
$$\theta' = -b_1 b_2 b_3 \left(\frac{s_1}{b_1^2} + \frac{s_2}{b_2^2} + \frac{s_3}{b_3^2}\right)\sin(\theta). \tag{2d}$$

While three distinct phases are present in the system, they appear only in the combination $\theta = \theta_1 + \theta_2 + \theta_3$, which we term the *combined phase*. The appearance of a combined phase (or *dynamic phase*, [14]) is typical of systems describing wave-wave interaction.

Both forms (1) and (2) of the problem will be used subsequently, and they shed light on different aspects of the system's behaviour. One important feature (cast in terms of (2)) is the invariant

$$I = b_1 b_2 b_3 \sin(\theta) = \Im(A_1 A_2 A_3), \tag{3}$$

which can be found by integrating the equation for the combined phase (for details see, e.g. Craik [13]).

3. Linear and quasilinear theory

Linearising equations (1) around the single-mode solution $A_1(t) = A_1(0)$, $A_2 = A_3 = 0$, yields the following system of equations

$$A_1' = 0, \tag{4a}$$
$$A_2' = s_2 A_1(0)^* A_3^*, \tag{4b}$$
$$A_3' = s_3 A_1(0)^* A_2^*. \tag{4c}$$

Note that this system reduces to

$$A_i'' = s_2 s_3 |A_1(0)|^2 A_i,$$

for $i = 2, 3$. The general solution can then be easily written as

$$A_{2,3} = C_{2,3}\exp(\sqrt{s_2 s_3}|A_1(0)|t) + D_{2,3}\exp(-\sqrt{s_2 s_3}|A_1(0)|t). \tag{5}$$

The coefficients $C_{2,3}$ and $D_{2,3}$ are determined by the initial conditions $A_2(0)$ and $A_3(0)$.

Separating the system (4) into amplitudes and phases yields the following quasi-linear system

$$b_1' = \theta_1' = 0, \tag{6a}$$
$$b_2' = s_2 b_1(0) b_3 \cos(\theta), \tag{6b}$$
$$b_3' = s_3 b_1(0) b_2 \cos(\theta), \tag{6c}$$
$$\theta' = -b_1(0)\left(\frac{s_2 b_3}{b_2} + \frac{s_3 b_2}{b_3}\right)\sin(\theta), \tag{6d}$$

where both b_1 and θ_1 are constants in accordance with the linearisation (4). Integration of Eq. (6d) shows that invariant (3) is unaltered for the linearised system. The behaviour of (6d) determines whether or not the phases "lock" on a single value, and will impact the subsequent distribution of the combined phase for random initial values.

If $s_2 s_3 > 0$ the system (4) is linearly unstable, and initially small modes grow exponentially, with a growth rate given by $\sqrt{s_2 s_3}|A_1(0)|$, as shown in (5). On the other hand, if $s_2 s_3 < 0$ the linear system (4) is stable, and the initially small modes remain small while undergoing oscillation. In this case A_2 and A_3 are periodic with period $2\pi/(\sqrt{s_2 s_3}|A_1(0)|)$.

3.1. Statistics for the linearised system

We are principally interested in exploring the statistics associated with the random phase model, whereby the initial amplitudes are given and each of the phases θ_1, θ_2 and θ_3 are independent and uniformly distributed random variables over $[-\pi, \pi]$. Each phase is also taken periodic with period 2π. Under these assumptions the combined phase $\theta = \theta_1 + \theta_2 + \theta_3$ is also uniformly distributed over $[-\pi, \pi]$ and periodic. We note that this is also the setting explored by Wilhelmsson & Östberg [5].

We focus on the time-evolution of θ, and also investigate the evolution of the moments of each of the complex amplitudes A_i for $i = 1, 2, 3$. The linear solution (5) can be used effectively in these computations.

3.1.1. Evolution of the moments

From Eqs. (4) and (5), and the fact that each individual phase θ_i has mean zero, it follows that $\langle A_i(t)\rangle = 0$, for each $i = 1, 2, 3$, where $\langle\cdot\rangle$ denotes the expected value.

For the evolution of the variances, which we relate to the energies of the modes, we start by computing $|A_i|^2$ from Eq. (5). Upon averaging the phases one obtains

$$\begin{aligned}\langle b_2^2\rangle = \langle |A_2|^2\rangle = &\frac{1}{2}\left(b_2^2(0) + \frac{|s_2|}{|s_3|}\frac{b_3^2(0)}{b_1^2(0)}\right)\cosh(2\Re(\sqrt{s_2 s_3})b_1(0)t)\\ &+ \frac{1}{2}\left(b_2^2(0) - \frac{|s_2|}{|s_3|}\frac{b_3^2(0)}{b_1^2(0)}\right)\cos(2\Im(\sqrt{s_2 s_3})b_1(0)t) \qquad (7)\\ \langle b_3^2\rangle = \langle |A_3|^2\rangle = &\frac{1}{2}\left(b_3^2(0) + \frac{|s_3|}{|s_2|}\frac{b_2^2(0)}{b_1^2(0)}\right)\cosh(2\Re(\sqrt{s_2 s_3})b_1(0)t)\\ &+ \frac{1}{2}\left(b_3^2(0) - \frac{|s_3|}{|s_2|}\frac{b_2^2(0)}{b_1^2(0)}\right)\cos(2\Im(\sqrt{s_2 s_3})b_1(0)t). \qquad (8)\end{aligned}$$

By inspection, we can conclude that in the unstable case ($s_2 s_3 > 0$) the variances grow exponentially, and in the stable case ($s_2 s_3 < 0$) they oscillate periodically and remain bounded.

3.1.2. Bicoherence

We are interested in the extent to which instability and the attendant change in modal amplitudes drives phase coherence in this system. For waves undergoing resonant energy exchange, the bispectrum is an effective way to characterise the degree of phase coherence, as described by Kim & Powers [15,16]. In our case the bispectrum is

$$B_{lin} = \langle A_1 A_2 A_3\rangle. \qquad (9)$$

The bispectrum must generally be calculated from (Fourier-transformed) measurements of a physical system, or via Monte-Carlo simulations, i.e. numerical solution of a system of equations with randomised initial conditions, and subsequent averaging. For the linearised system the solution (5) enables us to write an explicit expression for the bispectrum as a function of time in terms of the initial amplitudes:

$$B_{lin} = \frac{1}{2}b_1(0)\left(\sqrt{\frac{s_3}{s_2}}b_2^2(0) + \sqrt{\frac{s_2}{s_3}}b_3^2(0)\right)\sinh(2\sqrt{s_2 s_3}b_1(0)t). \qquad (10)$$

Note that B_{lin} is real regardless of linear stability or instability.

In addition to being a measure of phase coherence, the bispectrum also governs the evolution of the variances of A_2 and A_3. From averaging equation (6) it follows that for $i = 2,\ 3$

$$\frac{d}{dt}\left(\frac{1}{2s_i}\langle b_i\rangle^2\right) = \langle b_1 b_2 b_3\cos(\theta)\rangle = \Re\langle A_1 A_2 A_3\rangle = B_{lin}.$$

From the Cauchy–Schwarz Inequality

$$|B_{lin}|^2 = b_1^2|\langle A_2 A_3\rangle|^2 \le b_1^2\langle b_2^2\rangle\langle b_3^2\rangle,$$

and equality is obtained if and only if $A_2^* = \lambda A_3$, for some constant λ. In this case the phases are related through $\theta_2 = -\theta_3 - \arg(\lambda)$ and the combined phase is no longer random but is constant almost surely.

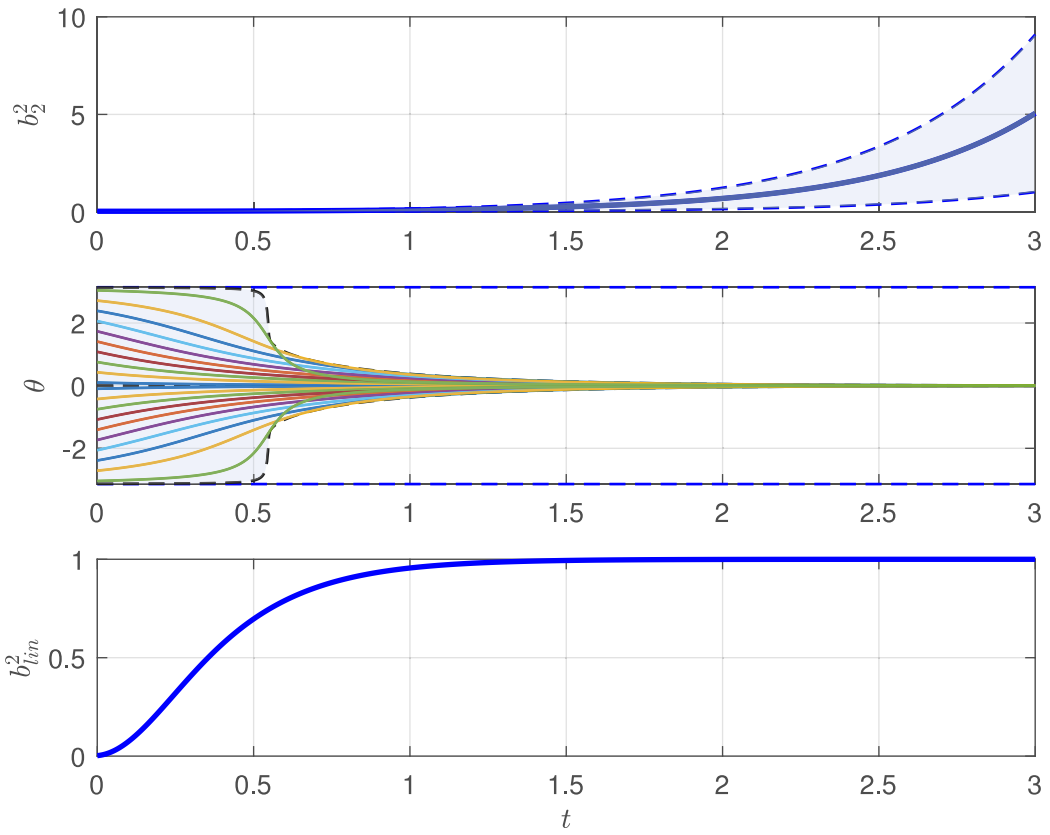

Fig. 1. Time evolution of a linearly unstable case with $s_1 = -1$, $s_2 = s_3 = 1$, $b_1 = 1$, $b_2(0) = 0.2$ and $b_3(0) = 0.1$. (Top panel) Plot of the squared amplitudes b_2^2 with time for different initial phases. The solid line is $\langle b_2^2 \rangle$; the envelope enclosed by the dashed lines contains all realisations from Monte-Carlo simulation with 1000 initial phases. (Middle panel) Plot of the combined phase with time with different initial conditions. Dashed lines corresponds to the trivial solutions $-\pi, 0, \pi$. (Bottom panel) Plot of the bicoherence with time. (For interpretation of the references to colour in this figure legend, the reader is referred to the web version of this article.)

Rather than employing the bispectrum directly it is useful to consider a normalised measure of phase coherence:

$$b_{lin}^2 = \frac{|B_{lin}|^2}{b_1^2 \langle b_2^2 \rangle \langle b_3^2 \rangle}, \tag{11}$$

which coincides with the bicoherence spectrum of [16]. It measures the degree of linear coupling between the phases of the waves, and varies between values of zero (no phase coherence) and one (perfect phase coherence).

3.1.3. Evolution of the statistics

To see the consequences of the foregoing theory, we consider two examples, in which the initial amplitudes are $b_1(0) = 1$, $b_2(0) = 0.2$ and $b_3(0) = 0.1$. We consider an unstable case with $s_1 = -1$, $s_2 = s_3 = 1$, and a stable case with $s_1 = s_2 = -1$, and $s_3 = 1$.

For the unstable system, regardless of the initial value of the combined phase, the two initially small modes b_2 and b_3 grow, as does their variance. This growth in the variance, exactly as captured by (7)–(8), is depicted in the top panel of Fig. 1, which shows mode b_2 only (mode b_3 is similar). The lighter shaded region shows the evolution of the deterministic mode amplitude squared $b_2(t)$ for 1000 realisations with random, uniformly distributed initial phases. The thick blue line shows the average of these realisations, i.e. the evolution of the variance. In each unstable realisation, as the modes b_2 and b_3 grow $\sin(\theta(t))$ must decay to conserve the invariant (3). Moreover, since the growth of b_2 and b_3 in the linearised setting is unbounded, $\sin(\theta(t))$ is forced to decay to zero. As 0 is the only attractor of the ODE (6d) over the interval $[-\pi, \pi]$, all the values of the phase $\theta(t)$ must tend to 0, irrespective of their initial value (the only exceptions are the unstable fixed points $\theta(0) = \pm\pi$). This is depicted in the middle panel of Fig. 1, which shows the evolution of 1000 initial phases $\theta(0)$ distributed over $[-\pi, \pi]$. The rapid approach of the combined phase to zero is termed *phase locking*.

The bottom panel of Fig. 1 shows the evolution of the bicoherence spectrum given by Eq. (11). As the phases lock, the bicoherence is observed to grow monotonically to one.

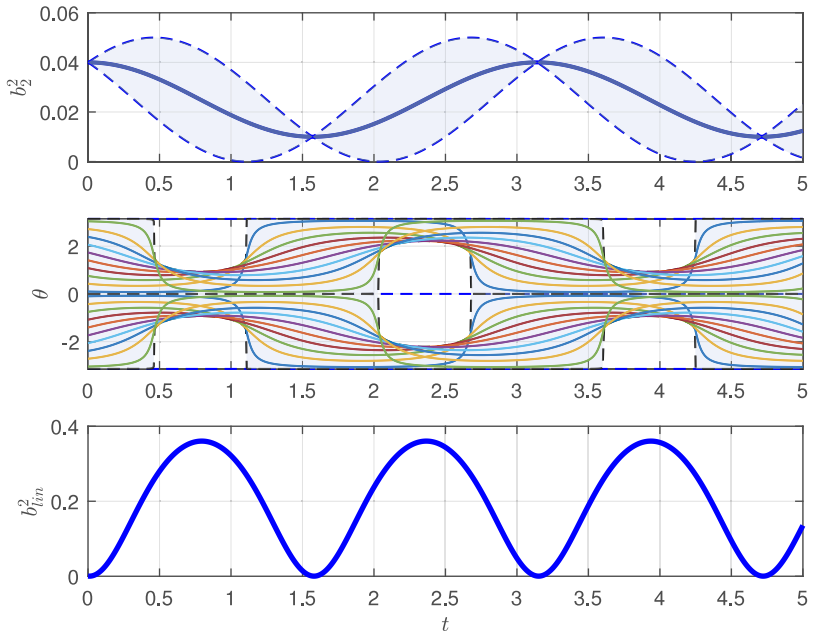

Fig. 2. Time evolution of a linearly stable case with $s_1 = -1$, $s_2 = -1$, $s_3 = 1$, $b_1 = 1$, $b_2(0) = 0.2$ and $b_3(0) = 0.1$. (Top panel) Plot of the squared amplitudes b_2^2 with time for different initial phases. The solid line is $\langle b_2^2 \rangle$; the envelope enclosed by the dashed lines contains all realisations from Monte-Carlo simulation with 1000 initial phases. (Middle panel) Combined phases θ with time for a stable case exhibiting *periodicity*. Dashed lines corresponds to the trivial solutions $-\pi, 0, \pi$. (Bottom panel) The bicoherence spectrum with time.

The corresponding results for our stable case are depicted in Fig. 2. In this case, the shaded region in the top panel shows the small, periodic oscillations of mode b_2 for 1000 uniformly distributed, random values of $\theta(0)$, together with the variance (solid line). As for the unstable case discussed above, modes b_1 and b_3 behave similarly, and are omitted from the plots for clarity. The variance oscillates at half the period of oscillation of b_2 and b_3, governed by the dominant mode amplitude $b_1(0)$, and the results of averaging again coincide with (7) and (8).

Rather than phase-locking, in the stable configuration the phase $\theta(t)$ returns periodically to its initial configuration, as shown in the middle panel of Fig. 2. In the bottom panel of Fig. 2 the bicoherence spectrum is seen to undergo periodic oscillations but shows no sign of phase coherence.

We have seen a surprising connection between instability and phase-locking for the linearised three-wave system. When the three initial phases are chosen randomly, this phase-locking (or coherence) has important consequences for the subsequent distribution of the phases. Kartashova and Bustamante [14,17] have shown the importance of taking the combined phase (also termed *dynamic phase*) into account in other three-wave problems, rather than equating it to a constant *a priori*. In fact, on short time-scales, the unstable system is insensitive to the choice of initial phases.

4. Nonlinear theory and long-time evolution

The linear theory presented above is sufficient to describe stable configurations, and sheds light on the initial evolution of unstable cases. The subsequent behaviour of such unstable triads must be treated within the fully nonlinear system (1). This treatment is simplified by exploiting an exact solution of the system, following the approach of Bretherton [18], Craik [13], or Kartashova [19].

4.1. Analytical solutions

The exact solution to the system is obtained by considering an auxiliary function $x(t)$, defined as the solution of the differential equation

$$x'(t) = \frac{d}{dt}\left(\frac{b_i^2}{s_i}\right) = 2b_1b_2b_3\cos(\theta), \quad \text{for } i = 1, 2, 3,$$

and with $x(0) = 0$. In terms of x the evolution of the amplitudes can be recovered from

$$b_i^2(t) = s_i x(t) + b_i^2(0), \quad \text{for } i = 1, 2, 3. \tag{12}$$

The auxiliary function itself satisfies the following equation

$$(x'(t))^2 = 4s_1s_2s_3\left(\Pi_{i=1}^3(x+c_i) - \Gamma\right) = 4s_1s_2s_3P_3(x), \tag{13}$$

where P_3 is the degree three polynomial

$$P_3(x) = \Pi_{i=1}^3(x+c_i) - \Gamma, \tag{14}$$

with $c_i = b_i^2(0)/s_i$ for $i = 1, 2, 3$, $\Gamma = c_1c_2c_3\sin^2(\theta) = I^2/(s_1s_2s_3)$, and I the invariant given in (3). The simplified form (13) is obtained from evaluation of the invariant at $t = 0$.

When one of the initial amplitudes is dominant, say $b_1(0) \gg b_2(0), b_3(0)$, P_3 has three real roots. This can be seen by introducing a small parameter ϵ so that $c_1 = O(1)$ and $c_2, c_3 = O(\epsilon)$ and expanding the discriminant Δ of P_3 up to order ϵ^2. The resulting expression is

$$\Delta = c_1^4c_2^2 + c_1^4c_3^2 + 2c_1^4c_2^2c_3^2(1 - 2\cos^2(\theta)) \geq c_1^4(c_2 - c_3)^2 > 0. \tag{15}$$

Furthermore, one of the roots is of order 1 (of the same order as the dominant amplitude $b_1(0)$) and the other two roots are of order ϵ, the same order of both $b_2(0)$ and $b_3(0)$.

The nonlinear differential equation (13) is separable, and leads to an elliptic integral involving the square root of the cubic on the right-hand side of (13). We present the explicit solution for both unstable and stable cases below.

4.1.1. Unstable case

The linearly unstable case where $s_2s_3 > 0$ contains two possibilities for the subsequent evolution: if the signs of all s_i are identical the instability is unchecked and solutions explode in finite time, otherwise the initial growth results in a periodic oscillation. We will focus on the latter case, whose subsequent time evolution is of interest.

Without loss of generality, let $s_1 < 0$ and $s_2, s_3 > 0$, as required for instability. In this case $P_3(0) = c_1c_2c_3\cos^2(\theta) < 0$ and the polynomial P_3 has three real roots $\beta_3 < \beta_2 < 0 < \beta_1$. Following [20], the solution of Eq. (13) is given by

$$x(t) = \beta_1 - (\beta_1 - \beta_2)\mathrm{sn}^2(\delta - ct, k), \tag{16}$$

where

$$\delta = \frac{1}{2}(\beta_1 - \beta_3)^{1/2}\int_0^{\beta_1}\frac{du}{\sqrt{-P_3(u)}}, \tag{17}$$

$$m = k^2 = \frac{\beta_1 - \beta_2}{\beta_1 - \beta_3}, \text{ and} \tag{18}$$

$$c = ((\beta_1 - \beta_3)|s_1s_2s_3|)^{1/2}. \tag{19}$$

Additional details regarding the computation of δ are given in Appendix A. Note that $x(t)$ is periodic with period

$$T = \frac{2}{((\beta_1 - \beta_3)|s_1s_2s_3|)^{1/2}}K(m), \tag{20}$$

where K denotes the complete elliptic integral of the first kind. Once $x(t)$ is determined, the evolution of $b_i(t)$ is recovered from Eq. (12) and the invariant can be used to find the combined phase $\theta(t)$.

4.1.2. Stable case

We leave $s_1 < 0$ as before and obtain a linearly stable case by either taking $s_2 < 0$ or $s_3 < 0$ but not both simultaneously. In either case $s_1s_2s_3 > 0$.

The main change is that the polynomial P_3 now has roots $\beta_3 < 0 < \beta_2 < \beta_1$ and $P_3(0) > 0$. Following [20], the exact auxiliary solution $x(t)$ is given by

$$x(t) = \beta_3 + (\beta_2 - \beta_3)\mathrm{sn}^2(\delta - ct, k), \tag{21}$$

where

$$\delta = \frac{1}{2}(\beta_1 - \beta_3)^{1/2}\int_{\beta_3}^{0}\frac{du}{\sqrt{P_3(u)}}, \tag{22}$$

$$m = k^2 = \frac{\beta_2 - \beta_3}{\beta_1 - \beta_3}. \tag{23}$$

The parameter c and period T are given be Eqs. (19) and (20), respectively.

Note that in the stable case the parameter m is small because the roots β_2 and β_3 are small with respect to β_1. This justifies approximating the period of $x(t)$ by $T \approx \pi/(b_1(0)\sqrt{s_2s_3})$, which is the period obtained from the stable linear solution. Moreover the amplitude of the oscillation is small because it is confined to the interval $[\beta_3, \beta_2]$.

4.2. Statistics of the nonlinear system

The most common approach to determining the statistics of a system such as (1) with random initial phases is Monte-Carlo simulation. In this fashion it is possible to obtain the behaviour of the moments and the bispectrum, and to identify phase-coherence or long-time behaviour for the full nonlinear system.

Despite its somewhat unwieldy form, the explicit solution (16) allows for direct insight into these statistics without the computational cost of Monte-Carlo simulations. This is particularly useful when studying the long time behaviour of the statistics. We will show that the moments and bispectrum can be obtained for arbitrary time by integration of the explicit solution.

Recall that the initial data consists of given complex amplitudes $A_1(0)$, $A_2(0)$ and $A_3(0)$. Their moduli are $b_i = |A_i|$ which are given positive constants. Randomness enters through their phases $\theta_i = \arg(A_i)$ which are uniformly distributed over $[-\pi, \pi]$ and the combined phase $\theta = \theta_1 + \theta_2 + \theta_3$ which, due to periodicity, also inherits the same initial distribution.

4.2.1. Evolution of the moments

As in the linearised setting presented in Section 3.1, $\langle A_i(t)\rangle = 0$ for $i = 1, 2, 3$ and all t, a fact that is independent of the stability or instability of the system. The proof of this fact is somewhat technical, and can be found in Appendix B.

The next quantities of interest are the variances of the complex amplitudes. These can be expressed in terms of the auxiliary function x by

$$\langle |A_i|^2\rangle = \langle b_i^2\rangle = s_i\langle x\rangle + b_i^2(0), \quad \text{for } i = 1, 2, 3. \tag{24}$$

Averaging over initial, uniformly distributed random phases reduces to evaluating the following integral

$$\langle x\rangle = \frac{1}{2\pi}\int_{-\pi}^{\pi} \beta_1 - (\beta_1 - \beta_2)\mathrm{sn}^2(\delta - ct, k)\, d\theta_0, \tag{25}$$

where all coefficients and parameters in these equation are function of the initial random variable $\theta(0) = \theta_0$, i.e. $c = c(\theta_0)$, $\beta_1 = \beta_1(\theta_0)$ and similarly for the remaining parameters. Finding δ as a function of θ_0 is a delicate matter because it involves inverting the periodic function sn. Further details on this matter are given in Appendix A, which includes, in Fig. A.8, a plot of δ as a function of θ_0. Since all the functions appearing in the integrals are periodic functions of θ_0, the trapezoidal rule with equally spaced points may be used to accurately compute this integral, and thus determine the variance at any time.

Moreover, using a procedure akin to that developed in [11, Appendix A], it can be shown that

$$\lim_{t\to\infty}\langle x(t)\rangle = \frac{1}{2\pi}\int_{-\pi}^{\pi}\frac{1}{T(\theta_0)}\int_0^{T(\theta_0)} x(s, \theta_0)\, ds d\theta_0. \tag{26}$$

In this equation T is the period given by Eq. (20). Recall that T and x depend on the initial phase θ_0, a fact that is highlighted by denoting these by $T(\theta_0)$ and $x(t, \theta_0)$. This allows the long-time asymptotics of the variance to be easily calculated.

4.2.2. Bicoherence

For the fully nonlinear problem we write the bicoherence spectrum as

$$b^2 = \frac{|\langle A_1A_2A_3\rangle|^2}{\langle |A_1|^2\rangle\langle |A_2A_3|^2\rangle}. \tag{27}$$

The numerator of Eq. (27) can be written as

$$\langle A_1A_2A_3\rangle = \langle x'\rangle,$$

where

$$x'(t) = 2c(\beta_1 - \beta_2)\mathrm{sn}(\delta - ct, k)\mathrm{cn}(\delta - ct, k)\mathrm{dn}(\delta - ct, k). \tag{28}$$

Its average is given by the following integral

$$\langle x'\rangle = \frac{1}{2\pi}\int_{-\pi}^{\pi} 2c(\beta_1 - \beta_2)\mathrm{sn}(\delta - ct, k)\mathrm{cn}(\delta - ct, k)\mathrm{dn}(\delta - ct, k)\, d\theta_0, \tag{29}$$

which is evaluated using the trapezoidal rule in the same way as for Eq. (25). This, together with (24), allows for explicit calculation of the bicoherence spectrum at arbitrary times.

As with the variance, we can establish a long-time asymptotic value for the bicoherence spectrum using the behaviour of x'. In this case

$$\lim_{t\to\infty}\langle x'(t)\rangle = 0, \tag{30}$$

from which it follows that the bicoherence spectrum decays to zero, i.e. phase coherence is lost for long times.

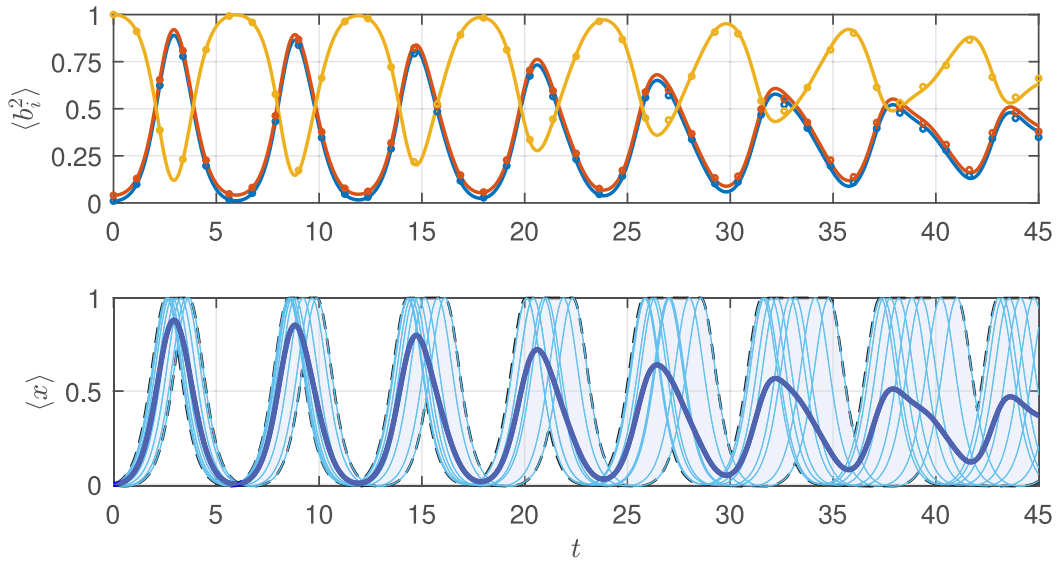

Fig. 3. Plot of variance $\langle b_i^2 \rangle$ (top panel) and average of the auxiliary variable $\langle x \rangle$ (bottom panel) with time for unstable initial conditions. (Top panel) Dots show the result of Monte Carlo simulations with 1000 random initial phases. Solid lines are computed from (25). (Bottom panel) The thin blue lines show the evolution of x for different values of the initial combined phase, with the shaded region containing all such values for $\theta(0) \in [-\pi, \pi]$. The thick blue line shows the average $\langle x \rangle$ (Monte Carlo simulations and (25) coincide). (For interpretation of the references to colour in this figure legend, the reader is referred to the web version of this article.)

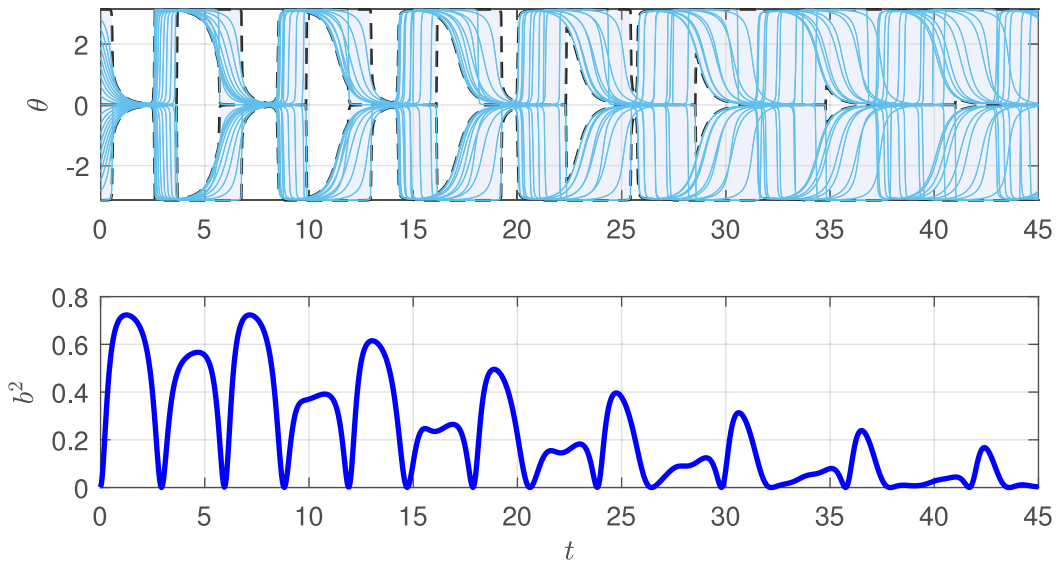

Fig. 4. Time evolution of the combined phase with initial conditions from $[-\pi, \pi]$ (top panel) and squared bicoherence (bottom panel) from unstable initial conditions. (Top panel) Thin blue lines show selected values of the combined phase, the shaded region contains all values of the combined phase for $\theta(0) \in [-\pi, \pi]$. (Bottom panel) The solid blue line shows the bicoherence spectrum (Monte Carlo simulations and calculation based on (29) coincide). (For interpretation of the references to colour in this figure legend, the reader is referred to the web version of this article.)

4.2.3. Evolution of the statistics

The theoretical results above provide insight into the statistics of linearly unstable initial conditions; the nonlinear evolution of linearly stable cases remains very similar to that discussed in Section 3.1. We shall study the fully nonlinear long-time behaviour of the two examples treated via linear theory in Section 3.1: the initial amplitudes are $b_1(0) = 1$, $b_2(0) = 0.2$ and $b_3(0) = 0.1$ and we consider an unstable case with $s_1 = -1$, $s_2 = s_3 = 1$, and a stable case with $s_1 = s_2 = -1$, and $s_3 = 1$.

The unstable system goes through three distinct stages in its evolution. Initially the energy (as measured by the variance $\langle b_i^2 \rangle$) of the small modes grows quickly at the expense of the dominant mode, exactly as predicted by the linear

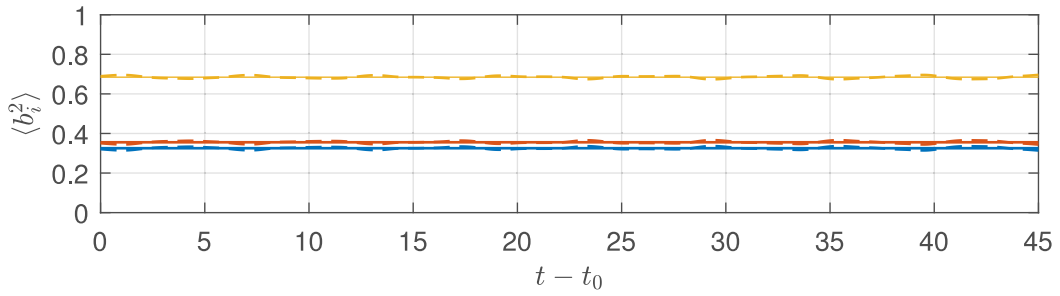

Fig. 5. Long-time behaviour of the moments $\langle b_i^2 \rangle$ for $i = 1, 2, 3$ for unstable initial conditions (as in Figs. 1–4). The dashed lines employ the expression (25) at long times. The solid lines use the asymptotic formula (26). The values of time start at $t_0 = 10^6$.

approximation, up to time $t \approx 2.5$, see Fig. 3. Subsequent to this initial growth, the system behaves in a recurrent fashion. This second stage of the evolution is also visible in Fig. 3 where we observe three, almost identical cycles, in the interval from $t = 0$ up to $t = 20$. For longer times, decay sets in; in Fig. 3 this begins after about $t = 25$ and persists throughout the subsequent evolution.

Fig. 4 shows the evolution of the combined phase and bicoherence spectrum for the unstable case, and helps to explain the behaviour observed in Fig. 3. In the top panel, the combined phase can be seen to tend quickly towards a fixed value irrespective of the initial condition; this coincides with a growth in the bispectrum shown in the bottom panel.

This phase-locking behaviour is governed by the ODE

$$\theta' = -b_1 b_2 b_3 \left(\frac{s_1}{b_1^2} + \frac{s_2}{b_2^2} + \frac{s_3}{b_3^2} \right) \sin(\theta) = \frac{x' x''}{\sqrt{x'^2 + 4I^2}} \sin(\theta), \tag{31}$$

where the last equality follows from Eqs. (12) and (13). Note that the auxiliary function x and its derivatives are periodic, depend on $\theta(0) = \theta_0$ and I is the invariant (3).

It is clear that $\theta(t) = n\pi$, with $n \in \mathbb{Z}$, are stationary solutions of Eq. (31). These fixed points either attract or repel the solutions depending on the sign of $x'x''/\sqrt{x'^2 + 4I^2}$; for a negative sign, fixed points of the form $n\pi$ with n even are attracting, whereas fixed points of the form $n\pi$ with n odd are repelling. When the sign of $x'x''/\sqrt{x'^2 + 4I^2}$ changes, the nature of the fixed points is reversed. The solution oscillates back and forth between 0 and π, or $-\pi$ and 0 depending of the sign of the initial condition. Note that the oscillation is due to the change in the attracting nature of the fixed points.

In contrast to the linearised system, the nonlinear phase-locking is not an end state; from time $t \approx 2.5$ in Fig. 3 the oscillation of the amplitudes changes the stability of the fixed-points, and initiates cycles of phase-locking which are eventually lost due to the distinct periods of each realisation. For longer times the values of θ are spread over the interval $[-\pi, \pi]$.

This phase behaviour is captured by the bicoherence spectrum b^2. From the lower panel of Fig. 4 one can see that values of b^2 close to one correspond to phase-locking, whereas the zeros of b^2 correspond to times where the values of θ are spread all over the interval $[-\pi, \pi]$. The gradual desynchronisation of the phases described above, is accompanied by decay in b^2.

For yet longer times Fig. 5 captures the decay of $\langle b_i^2 \rangle$, using the exact expression for the variance (25) (dashed lines) as well as the asymptotic value from (26) (solid lines). Here the phases have completely desynchronised, and the corresponding bicoherence spectrum tends to zero (see (30)). A similar computation shows that $\langle x(t)x'(t) \rangle$ tends to zero as t tends to infinity; meaning that the phases and the amplitudes become uncorrelated.

In the stable case the subsequent evolution remains close to the linear case; individual solutions undergo small, periodic oscillation around their initial values with periods given by (20). This behaviour comes from the exact solution $x(t)$ given by Eq. (21) and is plotted on the lower panel of Fig. 6.

A similar periodic pattern is observed in the combination of phases θ and the bicoherence spectrum b^2, both of which are plotted in Fig. 7. In the stable configuration we see that relatively larger values of b^2 correspond to instances where the values of θ do not span the entire interval $[-\pi, \pi]$ but lie on a small part of it and zeros of b^2 are found when the value of θ span the whole interval.

Despite the apparent recurrent behaviour of the stable case, the variance and bispectrum do undergo decay at very long time-scales; indeed, the fact that each realisation has a distinct period leads to eventual desynchronisation of the system. This is analogous to the unstable case described above, and leads to decay in both $\langle x(t) \rangle$ and b^2.

5. Discussion and conclusions

The resonant three-wave system (1), while ostensibly involving three amplitudes and three phases, depends only a single combined phase θ, which is the sum of the three phases involved. The equation connecting this combined phase and the amplitudes allows for the possibility of phase-locking or coherence, which coincides with the flow of combined

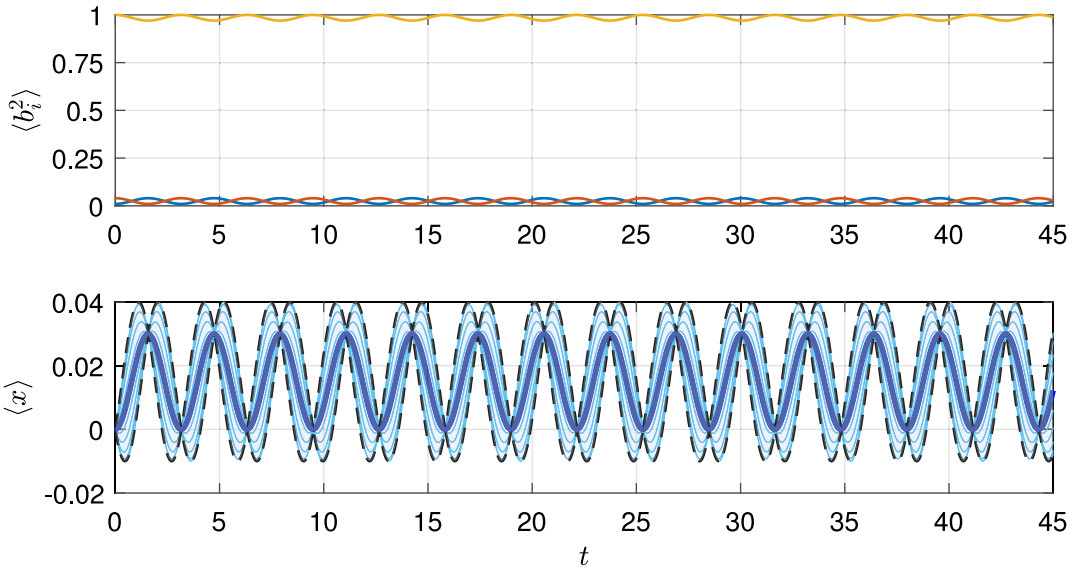

Fig. 6. Plot of variance $\langle b_i^2 \rangle$ (top panel) and average of the auxiliary variable $\langle x \rangle$ (bottom panel) with time for stable initial conditions. (Top panel) Plots of $\langle b_i^2 \rangle$ from Monte Carlo simulations with 1000 random initial phases. (Bottom panel) The thin blue lines show the evolution of x for different values of the initial combined phase, with the shaded region containing all such values for $\theta(0) \in [-\pi, \pi]$. The thick blue line shows the average $\langle x \rangle$ from Monte Carlo simulations. (For interpretation of the references to colour in this figure legend, the reader is referred to the web version of this article.)

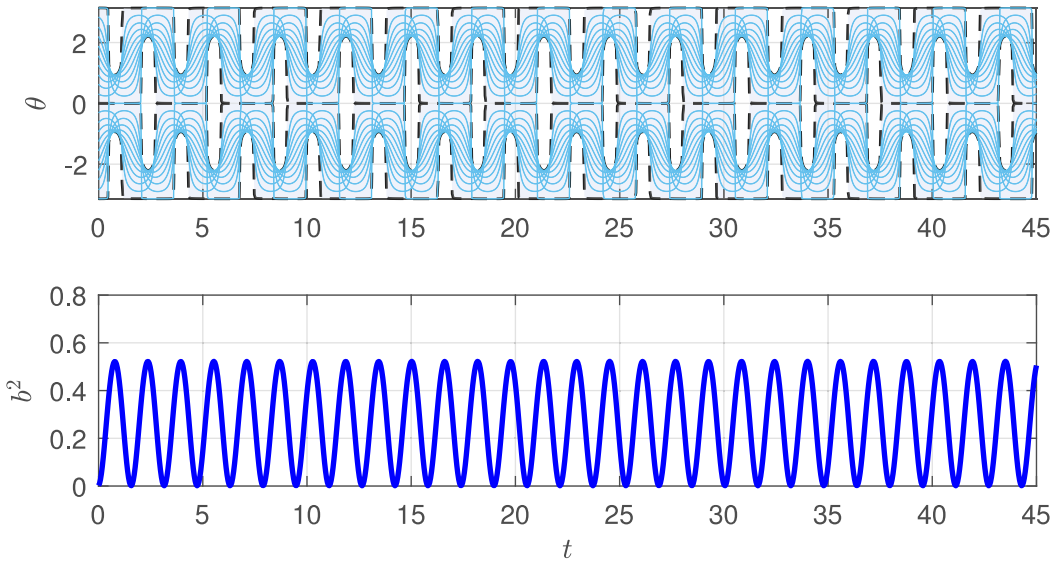

Fig. 7. Time evolution of the combined phase with initial conditions from $(-\pi, \pi)$ (top panel) and squared bicoherence (bottom panel) from stable initial conditions. (Top panel) Thin blue lines show selected values of the combined phase, the shaded region contains all values of the combined phase for $\theta(0) \in [-\pi, \pi]$. (Bottom panel) The solid blue line shows the bicoherence spectrum from Monte Carlo simulations. (For interpretation of the references to colour in this figure legend, the reader is referred to the web version of this article.)

phase towards the fixed points of the governing ODE. Such phase locking means that the combined phase tends to a fixed value irrespective of its initial value, which has important consequences for the statistics of the system with random phases.

By linearising the system about a single dominant mode we are able to easily identify stable and unstable initial conditions, as characterised by the sign of the coefficients s_i in Section 3. It is seen that instability coincides with phase locking — initially small modes growing as the combined phases become coherent. This phenomenon was also observed to occur in the linear stability analysis of a degenerate quartet of water waves [21]. In this case the linearising assumptions are soon violated, and the subsequent evolution must be studied via the fully nonlinear system.

While it is a simple matter to integrate this system numerically, we are helped by the existence of exact solutions in terms of Jacobi elliptic functions. These allow us to show explicitly that the time-evolution is periodic (with period given in (20) for the unstable and stable cases). The exact solutions also allow us to obtain direct insight into the statistics of the system with random phases, allowing for comparison with Monte-Carlo simulations as well as the derivation of long-time asymptotics.

When each mode of the three-wave system is treated as a stochastic process with random, uniformly distributed phases it is possible to develop a statistical theory. This includes an investigation of the mean, variance (related to the energy of the system in physical space), and bispectrum (a measure for correlation among the phases). For linearly stable systems, the mean of each mode is zero, while the variance is nearly constant; the degree of phase locking, as measured by the bispectrum, remains small.

Linearly unstable systems undergo fast initial phase locking, and show large, recurring fluctuations in the variance accompanied by a growth of the bicoherence spectrum. Cycles of coherence and decoherence alternate, and give way at long times to decay; the variance approaches a long-time asymptotic value calculated by means of the explicit solution, while the bispectrum approaches zero. We show results obtained both by Monte-Carlo simulation, as well as from compact explicit expressions.

Much of the results also apply to near-resonant triads, when a small detuning $\Delta = \omega_1 + \omega_2 + \omega_3$ is introduced into the three-wave system as follows:

$$
\begin{aligned}
A_1' &= s_1 A_2^* A_3^* e^{-i\Delta t},\\
A_2' &= s_2 A_1^* A_3^* e^{-i\Delta t},\\
A_3' &= s_3 A_1^* A_2^* e^{-i\Delta t}.
\end{aligned}
$$

This detuning introduces an additional constant term into Eq. (2d) governing the evolution of the combined phase. Increases in the magnitude of the detuning lead to stabilisation of the system and the disappearance of phase-locking effects.

While the system we have considered is deliberately simple, the connection between phase-locking and instability, as well as the link between fluctuations in the variance and the bicoherence spectrum, are likely to be of interest for other discrete resonant systems. Indeed, phase locking in the context of water waves has been associated with the phenomenon of crest enhancement by Houtani et al. [22], and was connected to the modulational instability by Liu et al. [21]. The consequent departure of the distribution of the combined phase from uniformity has been observed in Monte-Carlo simulations by Stiassnie & Shemer [11], who discussed it in the context of the applicability of phase-averaged theory. Having derived explicit expressions for variance, bispectrum, and their asymptotics, these should provide an important testing ground for such approximate theories. Moreover, understanding the simple building blocks – such as three-wave resonance – should provide valuable insight into more complex systems composed of many interacting triads.

CRediT authorship contribution statement

David Andrade: Conceptualization, Formal analysis, Investigation, Methodology, Writing – original draft, Writing – review & editing. **Raphael Stuhlmeier:** Conceptualization, Formal analysis, Funding acquisition, Investigation, Methodology, Writing – original draft, Writing – review & editing.

Declaration of competing interest

The authors declare that they have no known competing financial interests or personal relationships that could have appeared to influence the work reported in this paper.

Data availability

No data was used for the research described in the article.

Acknowledgements

This work was supported by EPSRC, UK project EP/V012770/1. The authors are grateful to the reviewers for a number of comments which improved and clarified the manuscript.

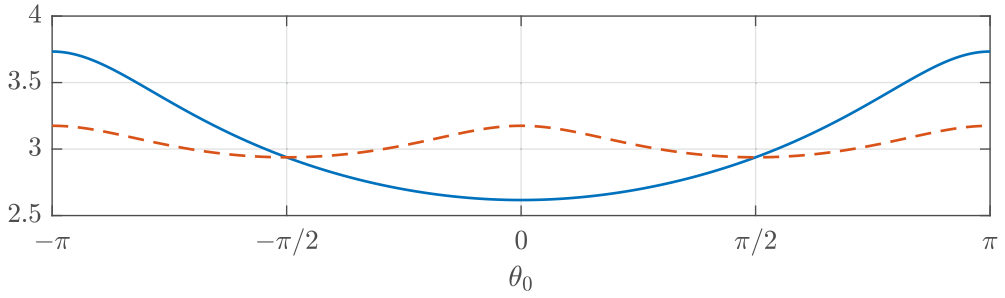

Fig. A.8. Blue solid line: Plot of the parameter δ as a function of the initial phase θ. Red dashed line: plot of the complete elliptic integral $K(m)$ as a function of θ_0, where $m = k^2$. Here $s_2 = s_3 = 1$, $s_1 = -1$, $b_1(0) = 1$, $b_2(0) = 0.2$ and $b_3(0) = 0.1$. (For interpretation of the references to colour in this figure legend, the reader is referred to the web version of this article.)

Appendix A. Computation of $\delta = \text{arcsn}\left((\beta_1/(\beta_1 - \beta_2))^{1/2}, k\right)$

The calculation of the auxiliary function $x(t)$ involves the computation of a parameter δ which appears as the solution of the equation

$$\text{sn}(\delta, k) = \sqrt{\frac{\beta_1}{\beta_1 - \beta_2}}. \tag{A.1}$$

The function sn is periodic. Therefore its inverse, the function arcsn, is a multiple-valued function and its inverse is only well defined on the interval $[-K, K]$, where $K = K(m)$ is the complete elliptic integral of the first kind with parameter $m = k^2$. The situation is analogous to that of the trigonometric function sin and its inverse arcsin.

For an initial $\theta(0) = \theta_0 \in [0, \pi/2]$, the values of k were computed directly from the roots of the polynomial P_3. We then used MATLAB's fsolve routine to compute δ. The initial guess for the numerical solver comes from the leading order terms of the Taylor expansion of arcsn computed by [23]

$$\text{arcsn}(z, k) = z + \frac{1}{6}(1 + k^2)z^3 + O(z^5), \tag{A.2}$$

evaluated at $z = \sqrt{\beta_1/(\beta_1 - \beta_2)}$. The resulting value satisfies the inequality $0 < \delta \leq K$ and only at $\theta_0 = \pi/2$ is equality achieved.

For $\theta_0 \in [\pi/2, \pi]$, the values of k are exactly the same as those computed for $\theta_0 \in [0, \pi/2]$. In this case we add $K(m)$ to the initial guess, computed through Eq. (A.2), so that the numerical solver will yield a result in the interval $[K, 2K]$. This delicate issue stems from the fact that the system of equations is not symmetric, i.e. the transformation $A_i \mapsto -A_i$ does not leave the system unchanged.

Lastly, due to the fact that the system of Eqs. (1) is symmetric with respect to complex conjugation, i.e. the transformation $A_i \mapsto A_i^*$ leaves the system unchanged, δ must be an even function of θ_0. This is used to obtain the values of δ over the interval $\theta_0 \in [-\pi, 0]$.

In Fig. A.8, the blue solid line is the plot of δ as a function of θ_0 and the red dashed line is K as a function of θ_0. Note that δ takes a different branch of the function arcsn at $\theta_0 = \pm\pi/2$.

Appendix B. Vanishing of first order moments

We shall prove that $\langle A_i \rangle = 0$, for all $i = 1, 2, 3$ and every $t \geq 0$. First, let $b_1, b_2, b_3 \geq 0$ be initial real amplitudes, $\phi_0 \in [-\pi, \pi]$ and denote by F_0 the set of all phases whose combination add up to ϕ_0, i.e.,

$$F_0 = \{(\phi_1, \phi_2, \phi_3) \in \mathbb{R}^3 \mid \phi_0 \equiv \phi_1 + \phi_2 + \phi_3 \ (\text{mod } 2\pi)\}. \tag{B.1}$$

Let A_1, A_2 and A_3 be the solution of Eqs. (1), corresponding to the initial conditions $A_i(0) = b_i e^{i\phi_i}$, for $i = 1, 2, 3$, where $(\phi_1, \phi_2, \phi_3) \in F_0$. Differentiating equations (1) with respect to t yields

$$A_1'' = A_1\left(s_1 s_2 |A_3|^2 + s_1 s_3 |A_2|^2\right). \tag{B.2}$$

$$A_2'' = A_2\left(s_2 s_3 |A_1|^2 + s_2 s_1 |A_3|^2\right). \tag{B.3}$$

$$A_3'' = A_3\left(s_3 s_1 |A_2|^2 + s_3 s_2 |A_1|^2\right). \tag{B.4}$$

The key observation is that $|A_1|^2$, $|A_2|^2$ and $|A_3|^2$ are the same functions for any choice of initial phases $(\phi_1, \phi_2, \phi_3) \in F_0$. This is because the evolution of $|A_i|^2$ only depends on the polynomial (14) which is the same for each triad of initial phases (ϕ_1, ϕ_2, ϕ_3), since $\phi_1 + \phi_2 + \phi_3 = \phi_0$.

Averaging equations (B.2) over the initial phases yields

$$\langle A_1\rangle'' = \langle A_1\rangle \left(s_1 s_2 |A_3|^2 + s_1 s_3 |A_2|^2\right). \tag{B.5}$$

$$\langle A_2\rangle'' = \langle A_2\rangle \left(s_2 s_3 |A_1|^2 + s_2 s_1 |A_3|^2\right). \tag{B.6}$$

$$\langle A_3\rangle'' = \langle A_3\rangle \left(s_3 s_1 |A_2|^2 + s_3 s_2 |A_1|^2\right). \tag{B.7}$$

We are taking the average A_i over all the possible ϕ, for $i = 1, 2, 3$, with $(\phi_1, \phi_2, \phi_3) \in F_0$. Note that the expression involving terms of the form $|A_i|^2$ can be pulled out of the average because they do not depend on the specific phases but rather on ϕ_0 which is fixed.

At $t = 0$ we have that

$$\langle A_i\rangle = \frac{1}{2\pi}\int_{-\pi}^{\pi} e^{i\phi_i}\, d\phi_i = 0 \quad \text{for } i = 1, 2, \tag{B.8}$$

$$\langle A_3\rangle = \frac{1}{2\pi}\int_{-\pi}^{\pi} e^{i\phi_3}\, d\phi_3 = \frac{1}{2\pi} e^{i\phi_0}\int_{-\pi}^{\pi}\int_{-\pi}^{\pi} e^{-i\phi_1} e^{-i\phi_2}\, d\phi_1 d\phi_2 = 0, \tag{B.9}$$

$$\langle A_i\rangle' = \frac{s_i}{2\pi} e^{-i\phi_0}\int_{-\pi}^{\pi} e^{i\phi_i}\, d\phi_i = 0 \quad \text{for } i = 1, 2, \tag{B.10}$$

$$\langle A_3\rangle' = \frac{s_3}{2\pi} e^{i\phi_0}\int_{-\pi}^{\pi}\int_{-\pi}^{\pi} e^{-i\phi_1} e^{-i\phi_2}\, d\phi_1 d\phi_2 = 0. \tag{B.11}$$

By uniqueness of solutions we must have that $\langle A_i\rangle = 0$, for all $t \geq 0$ and $i = 1, 2, 3$. Since the value of the initial phase combination ϕ_0 was arbitrary, it follows that $\langle A_i\rangle = 0$, for all $t \geq 0$ and $i = 1, 2, 3$, where the average is taken over all the possible initial phases.

References

[1] R.I. Ivanov, C.I. Martin, On the time-evolution of resonant triads in rotational capillary–gravity water waves, Phys. Fluids 31 (11) (2019) 117103.
[2] C.C. Chow, D. Henderson, H. Segur, A generalized stability criterion for resonant triad interactions, J. Fluid Mech. 319 (1972) (1996) 67–76.
[3] A. Constantin, E. Kartashova, Effect of non-zero constant vorticity on the nonlinear resonances of capillary water waves †, Europhys. Lett. 86 (2009) 29001.
[4] C.I. Martin, Resonant interactions of capillary–gravity water waves, J. Math. Fluid Mech. 19 (2017) 807–817.
[5] H. Wilhelmsson, K. Östberg, Phase-locking of coupled modes in nonlinearly unstable plasmas, Phys. Scr. 1 (5–6) (1970) 267–268.
[6] M. Longuet-Higgins, A. Gill, K. Kenyon, Resonant interactions between planetary waves, Proc. R. Soc. London. Ser. A. Math. Phys. Sci. 299 (1456) (1967) 120–144.
[7] P. Lynch, C. Houghton, Pulsation and precession of the resonant swinging spring, Phys. D Nonlinear Phenom. 190 (1–2) (2004) 38–62.
[8] M. Stiassnie, L. Shemer, On modification of the Zakharov equation for surface gravity waves, J. Fluid Mech. 143 (1984) (1984) 47–67.
[9] V.P. Krasitskii, On reduced equations in the Hamiltonian theory of weakly nonlinear surface waves, J. Fluid Mech. 272 (1994) 1–20.
[10] G.-b. Lin, H. Huang, Proof of six-wave resonance conditions of ocean surface gravity waves in deep water, China Ocean Eng. 33 (6) (2019) 734–738.
[11] M. Stiassnie, L. Shemer, On the interaction of four water waves, Wave Motion 41 (2005) 307–328.
[12] P.A. Janssen, The Interaction of Ocean Waves and Wind, Cambridge University Press, 2004.
[13] A.D.D. Craik, Wave Interactions and Fluid Flows, Cambridge University Press, 1986.
[14] M.D. Bustamante, E. Kartashova, Dynamics of nonlinear resonances in Hamiltonian systems, Europhysics 85 (1).
[15] Y.C. Kim, E.J. Powers, Digital bispectral analysis of self-excited fluctuation spectra, Phys. Fluids 21 (8) (1978) 1452–1453.
[16] Y.C. Kim, E.J. Powers, Digital bispectral analysis and its applications to nonlinear wave interactions, IEEE Trans. Plasma Sci. 7 (2) (1979) 120–131.
[17] M.D. Bustamante, E. Kartashova, Effect of the dynamical phases on the nonlinear amplitudes' evolution, Europhys. Lett. 85 (3).
[18] F.P. Bretherton, Resonant interactions between waves. The case of discrete oscillations, J. Fluid Mech. 20 (1964) 457.
[19] E. Kartashova, Nonlinear Resonance Analysis: Theory, Computation, Applications, Cambridge University Press, 2010.
[20] M. Abramowitz, I. Stegun, HandBook of Mathematical Functions with Formulas, Graphs, and Mathematical Tables, Dover Publications, New York, 1972.
[21] S. Liu, T. Waseda, X. Zhang, Phase locking phenomenon in the modulational instability of surface gravity waves, in: Proceedings of the 36th International Workshop on Water Waves and Floating Bodies, IWWWFB, Seoul, Korea, 2021, pp. 25–28.
[22] H. Houtani, H. Sawada, T. Waseda, Phase convergence and crest enhancement of modulated wave trains, Fluids 7 (8) (2022) 275.
[23] B.C. Carlson, Power series for inverse Jacobian elliptic functions, Math. Comp. 77 (263) (2008) 1615–1621.